Minerals Engineering 205 (2024) 108489

Contents lists available at ScienceDirect

Minerals Engineering

journal homepage: www.elsevier.com/locate/mineng

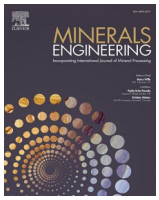

Mechanism and kinetic study of rare earth extraction from allanite by direct acid leaching

Wei Liu [a], Zhongqing Xiao [a], Subodh Das [b], Wencai Zhang [a,*]

[a] Department of Mining and Minerals Engineering, Virginia Polytechnic Institute and State University, Blacksburg, VA 24061, USA
[b] Phinix, LLC, Clayton, Missouri 63105, USA

ARTICLE INFO

Keywords:
Allanite
Rare earth elements
Acid leaching
Leaching kinetics
Activation energy

ABSTRACT

Direct acid leaching was conducted to recover rare earth elements (REEs) from an allanite ore assaying 9,861.4 ppm of REEs. The effects of operational variables, such as acid type, sulfuric acid (H_2SO_4) concentration, temperature, solid/liquid (S/L) ratio, and particle size, on the total REE (TREE) recovery were systematically examined. The REE mineralogy and the involved leaching mechanisms were investigated by electron microscopy characterization and residue re-leaching tests. It was found that approximately 80% of REEs was extracted using 1 M H_2SO_4 at 75 °C for 2 h. Increasing temperature significantly improved the REE extraction, while changing acid type, H_2SO_4 concentration, and particle size did not cause noticeable influences on the extraction efficiency. The low fraction of Si leached (<4.0%) suggested that the extraction did not significantly alter the crystal structure of the dominant minerals. The leaching kinetics of REEs was fast within the first 10 min, followed by a much slower stage (i.e., 10–120 min). The kinetic modeling results showed that both stages were likely controlled by both chemical reaction and diffusion, implying a mixed control mechanism. The activation energies for REE leaching using 1 M H_2SO_4 were determined to be 20.3 kJ/mol for the 0-10 min stage and 10.8 kJ/mol for the 10-120 min stage. The residue re-leaching results suggested that the initial fast leaching kinetics was caused by the preferential dissolution of metamict allanite, while the following slower leaching stage was due to the dissolution of difficult-to-leach REE-bearing minerals, such as well-crystallized allanite.

1. Introduction

Rare earth elements (REEs) were found to occur in approximately 270 minerals across the globe and 5 or 6 new rare earth minerals (REMs) are normally discovered each year (Brahim et al., 2022; Chakhmouradian and Wall, 2012). The major REE-bearing minerals are classified into silicates, carbonates, phosphates/oxysalts, and their corresponding fractions out of the total number of REMs are 43%, 23%, and 14%, respectively (Edahbi et al., 2019; Chakhmouradian and Wall, 2012). At present, the REMs with commercial significance are bastnasite ($RECO_3F$), monazite ($REPO_4$), xenotime (YPO_4), and ion adsorption clays (IACs), which account for ~95% of the total worldwide reserves of REEs (Gupta, 2021). However, the intensive growth of REE demands and the increasing depletion of conventional rare earth ores have fueled the urgency to identify secondary resources to ensure the security of REE supply chain (Leal Filho et al., 2023). Numerous alternative resources, such as low-grade rare earth minerals, mining waste, and electronic waste, have been considered potential feedstocks for REEs (Balaram; 2023; Edahbi et al., 2019).

Allanite, containing up to 51% REEs, is a rare earth silicate mineral of the epidote mineral group (Kursun et al., 2019). The ideal chemical formula of allanite may be written as $CaREEAl_2Fe(SiO_4)_3(OH)$ where REEs are incorporated into the crystal by means of the coupled substitution: $[Ca^{2+}][Fe^{3+}] \leftrightarrow [REE^{3+}][Fe^{2+}]$ (Gieré and Sorensen, 2004; Thibault and Gamage McEvoy, 2020). Besides REEs, the inclusion of large quantities of additional elements, such as Th, U, Zr, P, Ba, and Cr, in allanite had also been noticed (Jordens et al., 2014). Allanite mainly occurs as an accessory mineral in igneous, metamorphic, metasomatic, and sedimentary rocks, which are distributed in many parts of the world (Gupta and Krishnamurthy, 1992; Jordens et al., 2014). For instance, allanite in a micro-granite ore (Karan et al., 2022) and mylonitised metapelites (Akhila et al., 2022) has been found in Rajasthan and Singhbhum Shear Zone in India, respectively. Tzifas et al. (2019) and Benaouda et al. (2022) reported the existence of allanite in Mediterranean coastal sands in Northern Greece and pegmatites in the Ediacaran complex of Aghracha, South Morocco, respectively. Allanite does not

* Corresponding author.
E-mail address: wencaizhang@vt.edu (W. Zhang).

https://doi.org/10.1016/j.mineng.2023.108489
Received 16 August 2023; Received in revised form 29 October 2023; Accepted 31 October 2023

have economic significance like monazite, mainly due to the rare earth oxide (REO) content in allanite ore rarely exceeding 15 wt% and its resistance to chemical breakdown (Mariano and Mariano, 2012). However, according to Jackson and Christiansen (1993), three allanite deposits were considered to have the potential for mining. They are the uranium tailings at Mary Kathleen, Australia, the deposit in Alice Springs, Australia, and the deposits in Hall Mountain Group in Idaho, USA. The reserve of the allanite deposit in Alice Springs was estimated to 1 million metric tons with 4% allanite containing 20% REO. Allanite deposits available in large quantities enable them to be considered a critical rare earth resource in the future (Krishnamurthy and Gupta, 2015).

The extraction of REEs from the primary REMs starts with producing high-grade rare earth concentrates (30–92% in REO) using physical beneficiation technologies, such as froth flotation, to reduce the volume of materials subjected to the subsequent leaching step. Once the gangue minerals are removed, the REE concentrate is chemically leached using acidic or alkaline reagents to dissolve the REEs into solutions (Kim et al., 2016). Mineral acids, including sulfuric acid (H_2SO_4), hydrochloric acid (HCl), and nitric acid (HNO_3), are common lixiviants to leach REEs either directly from REE concentrates or from their pretreated products, such as REO and rare earth hydroxide ($RE(OH)_3$)). The direct leaching of REEs from monazite and bastnasite using acids has been thoroughly summarized by Kumari et al. (2015) and Cen et al. (2021). An indirect leaching process for monazite concentrate is to initially decompose it by 60–75% NaOH solution at elevated temperatures (120–150 °C), during which the refractory rare earth phosphate is converted to a readily leachable form (i.e., $RE(OH)_3$), which is then dissolved by acid. The selection of a decomposition method for a REM needs to evaluate its leachability and the possible influences of gangue minerals on the leaching performance (Kim et al., 2016).

The sulfuric acid baking process and direct H_2SO_4 leaching have been used to extract REEs from allanite (Demol et al., 2019). Baillie and Hayton (1970) studied the recovery of REEs from the allanite in Mary Kathleen uranium tailings via H_2SO_4 leaching and sulfuric acid baking. Around 65% of REEs can be dissolved by H_2SO_4 with unspecified concentration at 60% solid density and boiling temperature. H_2SO_4 leaching of an allanite concentrate from the Foxtrot deposit in Canada was carried out by Dreisinger et al. (2012). The results show that 95% of light REEs (LREEs) and 40–70% of heavy REEs (HREEs) were dissolved into the leachate with a free acidity of 0.93 M H_2SO_4. One issue involved in the two sulfuric acid baking processes is the co-extraction of significant amounts of Fe, Si, and Al. Karan et al. (2022) conducted direct acid leaching and aqueous leaching after sulfation roasting to recover REEs from a Bhatikhera micro-granite type ore containing 0.36% of TREE. It was found that aqueous leaching recovered 85% of TREEs and 75% of HREEs from the ground ore sample (<37 μm) after roasting at 300 °C for 3 h with a H_2SO_4 dosage of 250 kg/t. Moreover, Thibault and Gamage McEvoy (2020) performed sulfuric acid baking followed by water leaching to recover REEs from a Ce-type allanite. Experimental variables, such as baking temperature, acid concentration, and leaching temperature, were adjusted to minimize the formation of silica gel, which can inhibit the further decomposition of allanite. The results show that compared to the cases at 175–225 °C using concentrated H_2SO_4, the passivation effect resulting from the amorphous silica layers was less significant when the baking was conducted at 125 °C with 55% H_2SO_4 and the subsequent water leaching was performed at room temperature. Under those conditions, more than 90% of the REEs was recovered. It indicated that performing sulfuric acid baking at lower temperatures can help reduce the massive co-extraction of impure elements and energy consumption, enabling the leaching process to be more sustainable. However, to the best of our knowledge, information related to the leaching characteristics of REEs by acids from allanite collected from other places is limited, and the involved leaching kinetics was not clear.

The present study mainly aims to recover REEs from a US allanite ore using direct acid leaching at less than 100 °C. The emphasis here is sulfuric acid given it is the most common lixiviant being used in the minerals industry. The influences of operational factors, such as acid type, acid concentration, and temperature, on the leaching efficiency were evaluated. Electron microscopic characterization and leaching kinetic studies were conducted to better understand the decomposition behavior of allanite by H_2SO_4.

2. Experimental

2.1. Sample and reagents

An allanite ore collected from Halleck Creek, Wyoming, US was used as the feed sample for the extraction tests in this study. The as-received ore had been crushed into powders with 80% of the particles passing (i.e., d_{80}) 47.9 μm. Two representative splits from the feed were wet ground to d_{80} = 23.1 and 11.6 μm, respectively, using a planetary ball mill to determine the effect of particle size on the leaching performance. The elemental composition of the feed sample was determined by inductively coupled plasma mass spectrometry (ICP-MS) after being fused with lithium tetraborate at 1,000 °C for 15 min (Panteeva et al., 2003).

Trace metal-grade H_2SO_4 (98.0 wt%), HNO_3 (67.5 wt%), and HCl (34.0 wt%) purchased from Fisher Scientific were used for all the leaching experiments. Deionized (DI) water was used for the solution preparation and leaching tests.

2.2. Methods and procedures

2.2.1. Acid leaching tests

The feed samples were leached by acids to recover REEs. The effects of acid type (H_2SO_4, HNO_3, and HCl), initial H_2SO_4 concentration (0.5–1.5 M), particle size (d_{80} = 47.9, 23.1, and 11.6 μm, respectively), solid/liquid (S/L) ratio, and temperature (21–75 °C) on the leaching recovery were systematically examined to determine the optimal leaching conditions. The leaching tests were conducted in a 500 mL three-neck round-bottom flask connected to a condenser to minimize water evaporation during leaching. The flask was immersed in a water bath to maintain a constant leaching temperature. In each leaching test, 200 mL of the acid solution with a predetermined concentration was added to the flask and pre-heated to the desired temperature before mixing with 5.0 g of the sample. The slurry was magnetically agitated at 1,000 rpm for 2 h to provide adequate mixing. Representative samples (1.0 mL) of the slurry were withdrawn through a pipette at t = 1, 3, 5, 10, 15, 30, 60, 90, and 120 min, respectively, from the start of the leaching to monitor the leaching kinetics of REEs. After collecting each slurry sample, it was immediately centrifuged at 5,000 rpm for 5 min for solid–liquid separation. The REE contents in the supernatant were analyzed by ICP-MS after being diluted 100 times with a mixed acid solution (i.e., 2.5% HNO_3 and 0.5% HCl). After the leaching, the remaining slurry was collected into 50 mL centrifuge tubes and centrifuged at 5,000 rpm for 10 min. The centrifuge residue was collected, dried, weighted, and saved for further analysis. The volume of the supernatant was measured using a graduated cylinder. The leaching recovery of REEs was calculated according to Eq. (1),

$$R = 100 \times \frac{C_l V}{C_f M} \quad (1)$$

in which C_l and V are the REE concentration and volume of the leach liquor, respectively; and C_f and M are the REE concentration and weight of the feed sample, respectively. Each leaching test was repeated at least two times with the average result reported. The same procedure was used to re-leach the leaching residue to understand the leaching mechanisms. Before leaching, the residue was thoroughly rinsed with fresh DI water to minimize the interference of the residual REEs on the recovery.

2.2.2. Calcination

To examine the effect of calcination on the leaching recovery of REEs, the feed sample was calcined at different temperatures (i.e., 300, 600, and 900 °C) using a muffle furnace (EW-33858–80, Cole-Parmer, USA). A 10 g feed sample was placed in a 100 mL ceramic crucible, which was subsequently transferred to the muffle furnace. The calcination temperature was elevated from 25 °C at a ramping rate of 20 °C/min. The sample was calcined for 2 h after reaching the target temperature. After calcination, the furnace was naturally cooled to room temperature. Each calcinated product was leached by 1 M H_2SO_4 at 75 °C for 2 h according to the procedure mentioned in Section 2.2.1.

2.2.3. Sample characterization

X-ray diffraction (XRD) analysis was conducted to investigate the mineralogical changes of the feed sample before and after acid leaching. The analysis was conducted on a Bruker D8 Advanced Twin diffractometer with Cu-Kα radiation (Bruker Corporation, USA). Each sample was scanned over a 2θ range of 5°–70° with a step size of 0.02°. The XRD spectra were analyzed using the MDI Jade 6 software. The rare earth mineralogy of the feed sample and the leaching solid residue were characterized using scanning electron microscopy (SEM) equipped with energy dispersive spectroscopy (EDS) . The sample powders were sprinkled on double-sided carbon tape fixed on SEM stubs. Subsequently, the specimens were mounted on the sample holder and characterized by a JSM-IT500 SEM (JEOL Ltd., USA), which is in conjunction with an Ultim Max EDS detector (Oxford Instruments, UK). In addition, a Cameca SX-50 electron probe microanalyzer (EPMA, Cameca France) equipped with wavelength dispersive spectroscopy (WDS) was employed to determine the distribution of REE-bearing species in the feed sample. The same procedure as in the SEM analysis was used to prepare the specimen for the EPMA analysis.

3. Results

3.1. Sample characterization

Tables 1 and 2 show the elemental composition of REEs and other elements in the feed sample using the lithium tetraborate digestion method, respectively. The TREE content was assayed to be 9,861.4 ppm, of which the content of LREEs was much higher relative to HREEs, i.e., 9213.1 versus 648.3 ppm. Compared to other alternative rare earth sources, such as coal refuse, the high REE content in the feed sample enables it to be a promising REE feedstock.

Given the high REE assay, attempts were made to visualize the REE-bearing species in the feed sample using the EPMA-WDS technique. Fig. 1b-c show that over 50 discrete particles containing La, Nd, and Ce were found in the selected area (i.e., Fig. 1a). Those three REEs were detected since they were the three most abundant individual REEs compared to the remaining ones in the feed sample (see Table 1). It was found that the total amount of those three REEs accounted for 85.2% of the TREE content. The particle sizes of the REE-bearing particles were estimated to be <100 μm according to the scale bar. The occurrence of REEs as small and liberated particles can favor the leaching process due to the improved exposure of the particle surface to the lixiviant. Moreover, the REE-bearing particles with varying colors suggest that they had different REE contents, presumably resulting from their differences in mineralogical composition.

The results shown in Table 1 along with the EPMA-WDS mapping results show that most of the REEs should be associated with the LREE-enriched particles. According to the modal mineralogy study in the technical report (American Rare Earths, 2023), allanite, accounting for 93% of the REEs in the feed, was the dominant REM, while other REMs detected included synchysite/bastnasite ($CaCe(CO_3)_2F$, $Ce(CO_3)F$) and chevkinite/tornebohmite ($(Ce_4(Ti,Fe^{2+},Fe^{3+})_5O_8(Si_2O_7)_2$, $Ce_2Al(SiO_4)_2(OH)$). The feed sample used in this study was collected from the same source as the one characterized in the report (American Rare Earths, 2023). It is, therefore, reasonable to assume that they had similar REE mineralogy, which was further corroborated by the SEM characterization in the current study. Fig. 2 shows the backscattered electron images and corresponding EDS spectra of three REE-bearing particles. The EDS spectra suggest that the three particles were more likely to be an allanite (a_1), a synchysite/bastnasite (b_1), and a chevkinite/tornebohmite (c_1) particle, respectively. Several other allanite-like particles had been found (not shown). The SEM characterization along with the findings in the report (American Rare Earths, 2023) indicates that allanite was the dominant REM in the feed sample , while synchysite/-bastnasite and chevkinite/tornebohmite were in minor amounts.

The major elements (i.e., ≥1%) in the feed sample were Si, Al, Na, K, and Fe (see Table 2), of which Si, Fe, and K were found in the EMPA maps shown in Fig. 1. It reveals that the dominant minerals in the feed sample were silicates, which is consistent with the XRD analysis shown in Fig. 6. It shows that albite ($NaAlSi_3O_8$), microcline ($KAlSi_3O_8$), and actinolite ($Ca_2(Mg_{4.5\text{-}2.5}Fe^{2+}_{0.5\text{-}2.5})Si_8O_{22}(OH)_2$) were the dominant crystalline minerals in the feed sample. XRD was not able to detect the REE-bearing minerals since the REE content was lower than the detection limit of XRD (~1% by volume).

3.2. Leaching tests

3.2.1. Effect of acid type on the TREE recovery

A series of direct acid leaching tests were conducted to recover REEs from the feed sample and determine the optimal leaching conditions. Fig. 3 shows the effects of acid type, initial H_2SO_4 concentration, particle size, S/L ratio, and leaching temperature on the TREE recovery from the feed sample. The feed sample with a d_{80} of 47.9 μm was leached by different acids at 75 °C for 2 h with a S/L ratio of 25 g/L. It can be seen in Fig. 3a that 1 M HCl and HNO_3 obtained similar final TREE recoveries (~73.0%), which were lower than that of 0.5 M H_2SO_4 by four absolute percentage points. This comparison suggests that the latter was more effective relative to the former two acids. Since the hydrogen concentrations of those three acids were the same (i.e., 1 M), the superior leaching performance of H_2SO_4 relative to the other two may be explained by their differences in the stability constants of rare earth complexes. The stability constants (i.e., Log K = 3.01 to 3.37) of $RESO_4^+$ are two to three orders of magnitude larger than those of $RENO_3^{2+}$ (log K = 0.15 to 0.88) and $RECl^{2+}$ (Log K = -0.03 to 0.32) (Millero, 1992). Compared to NO_3^- and Cl^-, the stronger complexing ability of SO_4^{2-} enables RE^{3+} to exist as more stable complexes in the leaching solution, contributing to the continuous removal of the reaction products (i.e., RE^{3+} ions) from the reaction system. As such, the dissolution reaction of the rare earth minerals can move forward (Moldoveanu and Papangelakis, 2012; Liu et al., 2022). The results presented in Fig. 3a show that H_2SO_4 is the most effective lixiviant. On the other hand, H_2SO_4 is a popular lixiviant due to its lower cost and lower volatility relative to HCl

Table 1
TREE and individual REE contents in the feed sample (in ppm) determined by inductively coupled plasma mass spectrometry (ICP-MS). LREEs include Sc, La, Ce, Pr, Nd, and Sm; HREEs contain Y, Eu, Gd, Tb, Dy, Ho, Er, Tm, Yb, and Lu.

TREE	Sc	Y	La	Ce	Pr	Nd	Sm	Eu	Gd
9861.4	33.5	275.0	2163.1	4348.6	508.7	1891.5	267.7	15.5	174.1
Tb	Dy	Ho	Er	Tm	Yb	Lu	LREEs	HREEs	
18.9	86.6	14.0	31.0	4.4	24.9	4.0	9213.1	648.3	

Table 2
The content of other elements in the feed sample (in ppm) determined by ICP-MS.

Na	Mg	Al	Si	P	K	Ca	Ti
32193.6	3090.1	86980.7	260939.5	5390.9	38697.5	9766.7	6519.2
Fe	Mn	Cu	Zn	Ba	Th	U	
77871.6	1623.5	802.4	540.0	1186.1	194.2	13.6	

and HNO_3 (Yu et al., 2013; Yang and Honaker, 2020). Therefore, H_2SO_4 will be used as the lixiviant for the rest of the leaching tests in this study.

3.2.2. Effect of the initial H_2SO_4 concentration on the TREE recovery

Fig. 3b shows the effect of the initial H_2SO_4 concentration on the TREE recovery. The feed sample with a d_{80} of 47.9 μm was leached by H_2SO_4 at 75 °C for 2 h with a S/L ratio of 25 g/L. As the acid concentration varied from 0.5 to 1.5 M, the final TREE recovery increased from 76% to 83%. There was only a 6% improvement in the recovery, suggesting that increasing the acid concentration slightly enhanced the dissolution of the REE-bearing minerals in the feed sample. The 76% TREE recovery obtained by 0.5 M H_2SO_4 suggested that the majority of the REMs were amenable to acid leaching. They may be allanite and bastnasite with poor crystallinity. According to Thibault and Gamage McEvoy (2020), the chemical reaction for allanite dissolution can be written as reaction (2), in which REEs and other metals are dissolved into their sulfates. All other sulfates are water soluble except $CaSO_4$ which may form a precipitate. However, the remaining REMs may be well-crystallized and/or poorly liberated, which were more resistant to acid leaching. Therefore, a limited beneficial effect was achieved by increasing the acid concentration. A detailed explanation of the REMs especially allanite with varying crystallinities is provided in Section 4.2. Given the limited benefit from 1.5 M H_2SO_4, 1.0 M was considered the optimal concentration for H_2SO_4 leaching in this study.

$$CaREEAl_2Fe(SiO_4)_3(OH) + 6.5H_2SO_4 \rightarrow CaSO_4 + FeSO_4 + Al_2(SO_4)_3 + 0.5REE_2(SO_4)_3 + 3SiO_2 + 7H_2O \quad (2)$$

3.2.3. Effect of particle size on the TREE recovery

The motivation of this section is to investigate whether the physical liberation of REMs can affect the TREE recovery by reducing the particle size of the feed sample. The feed samples with three different d_{80} were subjected to 1 M H_2SO_4 leaching at 75 °C for 2 h with a S/L ratio of 25 g/L. The results in Fig. 3c show that the final TREE recovery slightly increased from 80% to 82% when the d_{80} decreased from 47.9 to 11.6 μm. The leaching curves of the samples with d_{80} = 23.1 and 11.6 μm were nearly identical, suggesting that a complete recovery of REEs from the feed sample is hard to achieve only by grinding under the experimental conditions explored. The only benefit resulting from the grinding was the faster leaching kinetics. In the first 15 min, the TREE recoveries of the samples with finer particle sizes were 5 to 11 absolute percentage points higher relative to the unground sample (i.e., the one with d_{80} = 47.9 μm). After 15 min, the discrepancy in the recovery gradually diminished. Particle size has been found to be an important experimental variable that can affect the leaching recovery. Yang and Honaker (2020) concluded that there may be two advantages that can be obtained by grinding the coal-based clay for REE extraction. One is the improved mineral liberation and the creation of more surface area, which enhances the interaction between mineral surface and lixiviants. The other one is the release of REMs and RE oxides in nano size. However, the above results demonstrated that reducing particle size slightly facilitated the leaching performance. As such, physical liberation was less likely to be the main reason for the incomplete leaching of REEs.

3.2.4. Effect of S/L ratio on the TREE recovery

S/L ratio is a variable that evaluates the treatment capacity of a leaching agent (Mao et al., 2022). Conducting metal extraction at a higher S/L ratio means greater utilization of a lixiviant, assuming similar leaching recoveries are obtained during the leaching process. In this work, the S/L ratio was varied from 25 g/L to 200 g/L to evaluate its impact on the leaching performance. Fig. 3d shows that the TREE recovery with the use of 1 M H_2SO_4 gradually reduced from 80% to 46% with the increase of S/L ratio. It indicated that higher S/L ratio had a negative effect on the leaching performance. At the higher S/L ratios, the increased amount of gangue minerals consumed more acid, resulting in an insufficient amount of the lixiviant available for the further dissolution of the REE-bearing minerals, such as allanite. On the other hand, increasing S/L ratio resulted in weaker interactions between lixiviants and the target sites where REEs exist, thereby leading to poorer leaching efficiencies.

3.2.5. Effect of temperature on the leaching of REEs and contaminant elements

The influence of leaching temperature on the TREE recovery was conducted on the feed sample with a d_{80} of 47.9 μm by 1 M H_2SO_4 at various temperatures (21–75 °C) for 2 h with a S/L ratio of 25 g/L. 21 °C was the actual temperature measured for the leaching test conducted at room temperature. The results presented in Fig. 3e show that the final TREE recovery gradually increased from 49% to 80% as the temperature varied from 21 to 75 °C. Temperature facilitated the REE extraction may be through enhancing the reaction rate and the diffusion rate of the reactants (Li et al., 2017). On the other hand, the initial leaching rate of REEs (i.e., 0–10 min) was more sensitive to temperature compared to the subsequent leaching rate at each temperature. However, it should be noticed that the discrepancy between the leaching curves obtained at 65 to 75 °C was smaller relative to other cases, indicating that further increasing the leaching temperature beyond 75 °C may not be necessary given the limited revenue.

Fig. 4 shows the responses of the final REE recovery (at t = 120 min) to the temperature elevation. Although the recovery of each REE gradually increased with temperature, the increases depended on specific elements. From 21 to 75 °C, the recoveries of REEs located from La to Sm increased to greater extents relative to those from Gd to Lu. Moreover, it was noticed that the recoveries of HREEs especially from Dy to Lu gradually decreased with the atomic number at each temperature. It indicates that LREEs were more preferentially extracted relative to HREEs. The recoveries of Sc were <11% at all temperatures, which may be attributed to its association with acid-resistant minerals, such as insoluble silicates. Eu also had a relatively lower recovery, possibly due to its unstable chemical property (Liu et al., 2022).

The leaching characteristics of contaminant elements, such as Al, Si, Fe, Ca, K, and Na, in the sulfuric acid leaching tests conducted at different temperatures were also investigated to evaluate the dissolution of the gangue minerals. Fig. 5 shows the fractions of those six contaminant elements leached at different temperatures. It was noticed that except for Fe, the fractions of other impurities leached were around or less than 10% and were slightly affected by temperature. The fractions of Si, Na, and K extracted immediately reached their corresponding maximum values with the first 10 mins and leveled off thereafter. The low fractions of Si, Na, K, and Al leached indicated that the decomposition of the dominant minerals was not significant. The leaching residues obtained at 35, 55, and 75 °C were characterized by XRD to identify the possible phase transformations during the H_2SO_4 leaching. It was observed in Fig. 6 that the leaching residues had similar XRD patterns compared to the feed sample except for the reduced intensity of the

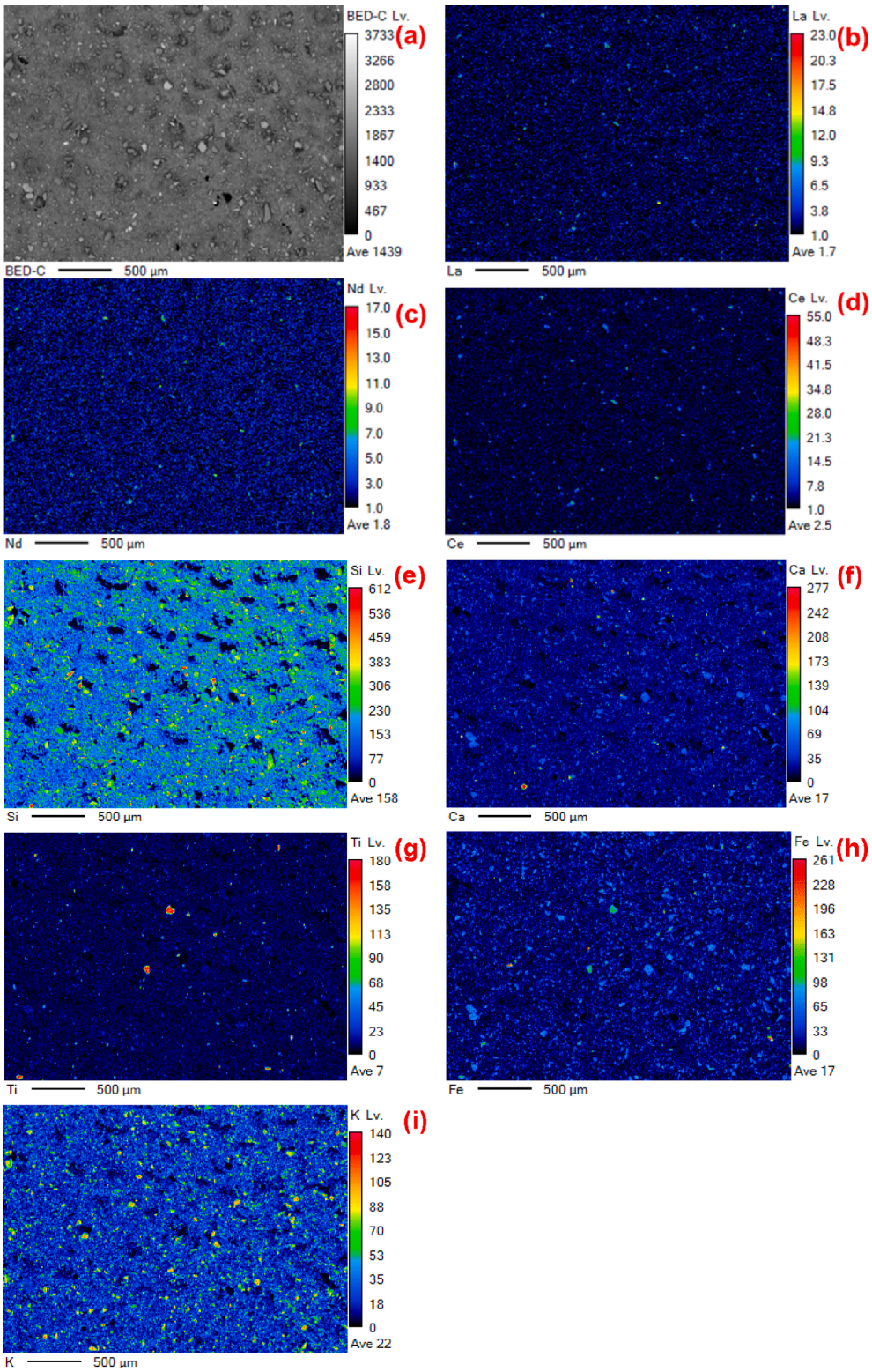

Fig. 1. Backscattered electron image (a) and compositional mapping of La (b), Nd (c), Ce (d), Si (e), Ca (f), Ti (g), Fe (h), and K (i) of a selected area from the feed sample by electron probe microanalyzer-wavelength dispersive spectroscopy.

peaks. Albite and microcline were still the dominant minerals in the residue and no new species were detected. The involved chemical reactions for the dissolution of albite and microcline by H_2SO_4 may be written as reactions (3) and (4), respectively. It is true that the dissolution of the dominant minerals was responsible for the reduced peak intensity. However, the low Si recovery revealed that the decomposition was limited. Therefore, another reason for the reduced peak intensity may be the alteration of the crystallinity of the dominant minerals during the leaching process.

$$2NaAlSi_3O_8 + 4H_2SO_4 + 8H_2O \rightarrow Al_2(SO_4)_3 + 6H_4SiO_4 + Na_2SO_4 \quad (3)$$

$$2KAlSi_3O_8 + 4H_2SO_4 + 8H_2O \rightarrow Al_2(SO_4)_3 + 6H_4SiO_4 + K_2SO_4 \quad (4)$$

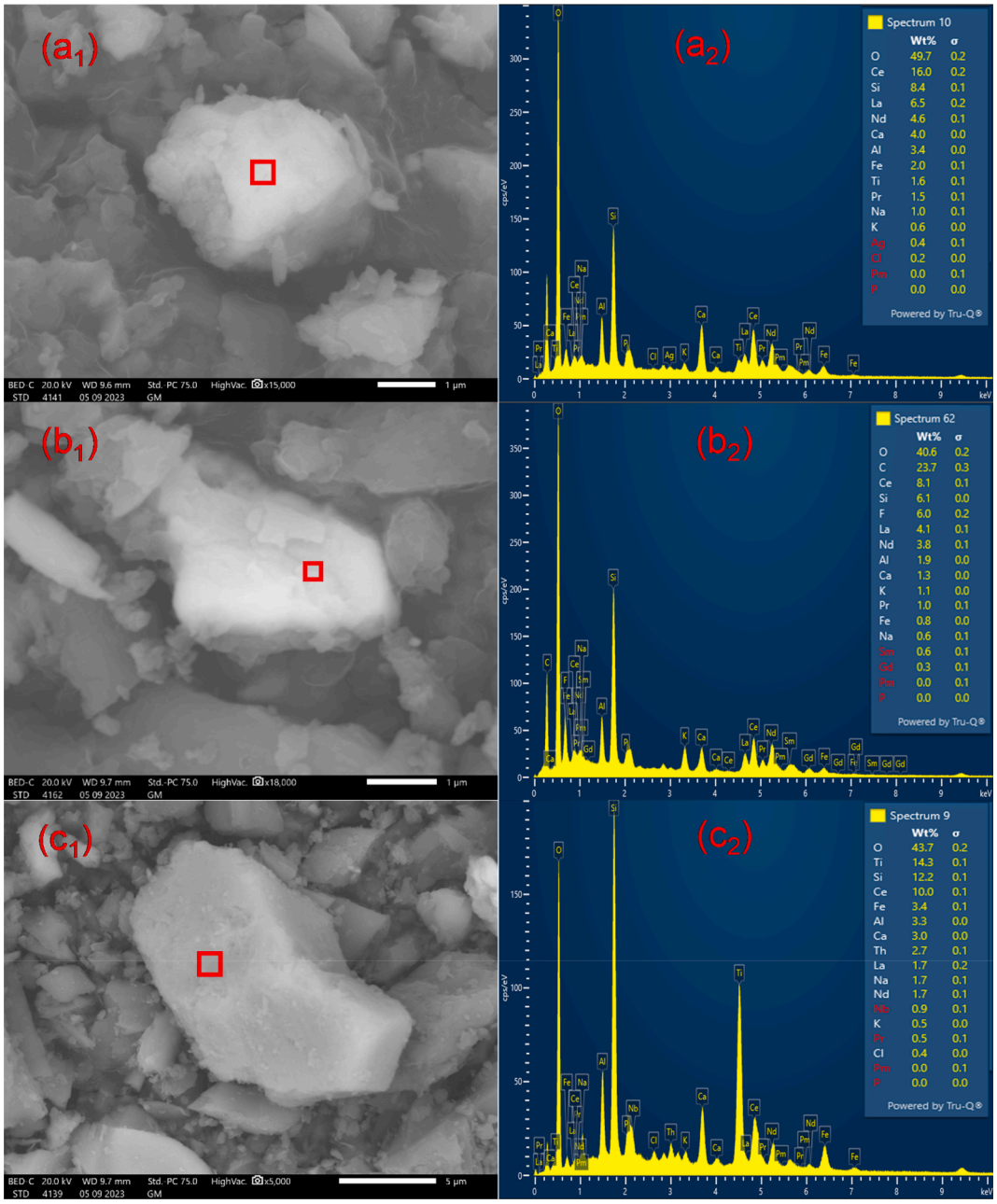

Fig. 2. Backscattered electron images and their corresponding energy dispersive spectroscopy (EDS) spectra of the selected areas in allanite (a_1 and a_2), synchysite/bastnasite (b_1 and b_2), and chevkinite/tornebohmite (c_1 and c_2) particles found in the feed sample.

Table 2 shows that the content of Fe in the sample was 7.8%, but XRD did not detect any individual Fe-enriched minerals. However, the SEM characterization of the current study along with the findings in the report (American Rare Earths, 2023) show that Fe existed as Fe-(Ti) oxides and substituted components in other minerals, such as asteroite, i.e., (Ca, Na)(Mg,Fe^{2+},Al,Fe^{3+},Ti)[$(Si,Al)_2O_6$], and allanite in the feed sample. Fig. 5c shows that the fraction of Fe leached ranged from 31% to 42% when the temperature varied from 21 °C to 75 °C. Unlike the other contaminant elements (e.g., Si, Na, and K), Fe had a relatively slower leaching kinetics at each temperature. The distinct leaching behavior of Fe may suggest that it had a different association with Si, Na, and K. Results in this section show that the dissolution of the gangue minerals was not significant during the acid leaching process.

3.3. Kinetic analysis of the H_2SO_4 leaching

Fig. 3 shows that the leaching curves of REEs share a common characteristic. All the curves can be divided into two parts: a rapid leaching at the beginning followed by a slower leaching process. To gain insights into the mechanisms controlling the leaching rate of REEs, the leaching kinetics was modeled according to the shrinking core model, a classical model that has been used to describe the leaching process of non-porous particles (Georgiou and Papangelakis, 1998). The model is divided into the following independent models (Li et al., 2013; Brahim et al., 2022):

Chemical reaction controls:

$$1-(1-x)^{\frac{1}{3}}=k_1 t \tag{5}$$

Outer diffusion controls:

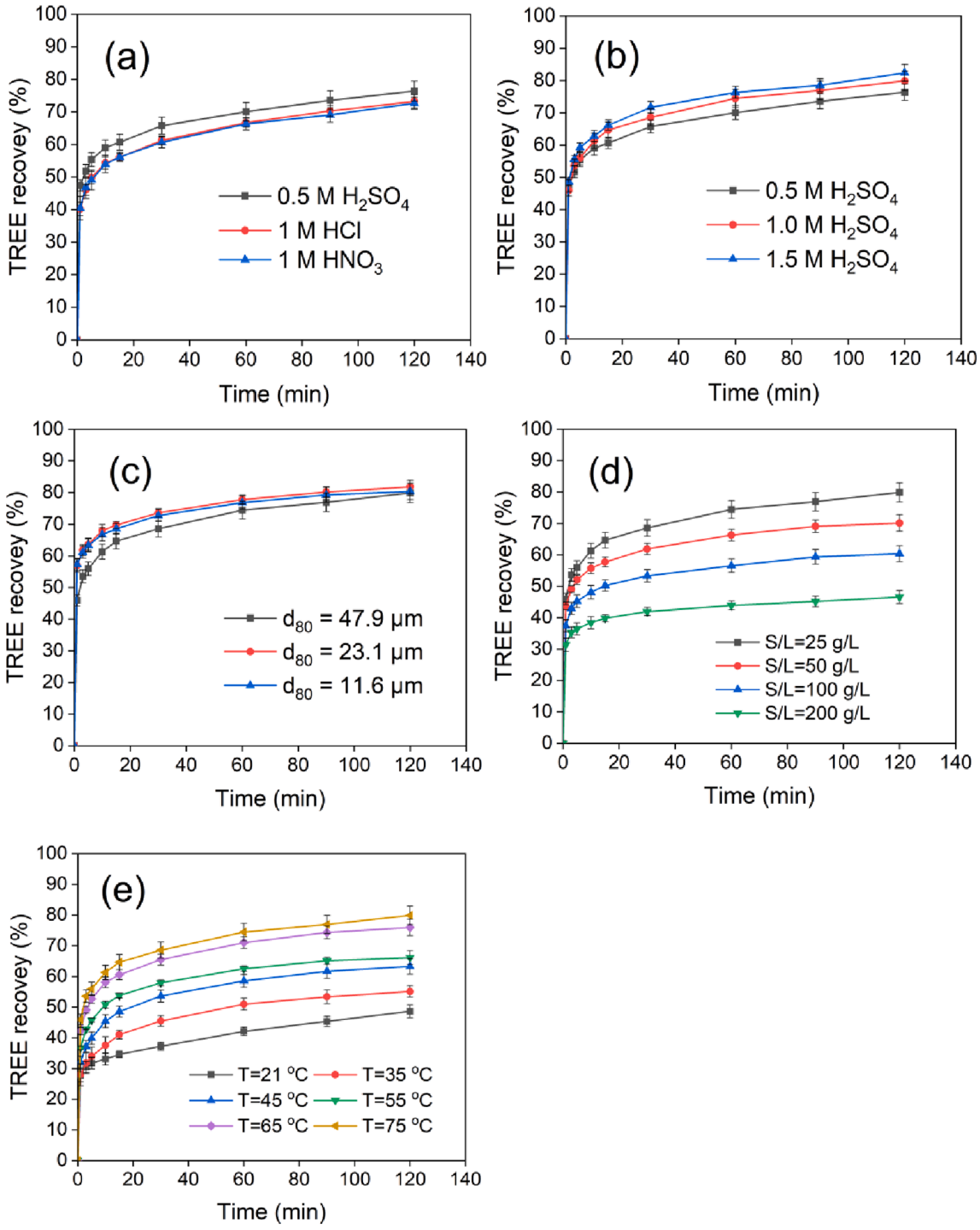

Fig. 3. Effects of acid type (a), initial sulfuric acid (H_2SO_4) concentration (b), particle size (c), solid/liquid (S/L) ratio (d), and leaching temperature (e) on the total rare earth element (TREE) recovery from the feed sample. Conditions for the tests in (a) and (b): S/L ratio = 25 g/L, 75 °C, 2 h, and d_{80} = 47.9 μm; conditions for the tests in (c): 1 M H_2SO_4, S/L ratio = 25 g/L, 75 °C, and 2 h; conditions for the tests in (d): 1 M H_2SO_4, d_{80} = 47.9 μm, 75 °C, and 2 h; conditions for the tests in (e): 1 M H_2SO_4, d_{80} = 47.9 μm, 75 °C, S/L ratio = 25 g/L, and 2 h. Note: error bars represent the standard deviations.

$$1-(1-x)^{\frac{1}{3}}=k_2t \tag{6}$$

Inner diffusion controls:

$$1-\frac{2}{3}x\text{-}(1-x)^{\frac{2}{3}}=k_3t \tag{7}$$

Mix controls:

$$1-(1-x)^{\frac{1}{3}}+\mathrm{B}[1-\frac{2}{3}x\text{-}(1-x)^{\frac{2}{3}}]=k_4t \tag{8}$$

$$k=Aexp(-\frac{E_a}{RT}) \tag{9}$$

where k_1, k_2, k_3, and k_4 are the apparent reaction rates (min^{-1}) for different control steps, respectively; x is the fraction of REEs extracted at time t (min); B is defined as the ratio of k_1/k_3. The Arrhenius equation used to determine the activation energy (E_a) is shown in Eq. (9), where k, A, R, and T are the rate constant (min^{-1}), pre-exponential factor, universal gas constant (8.413 J mol^{-1} K^{-1}), and absolute temperature

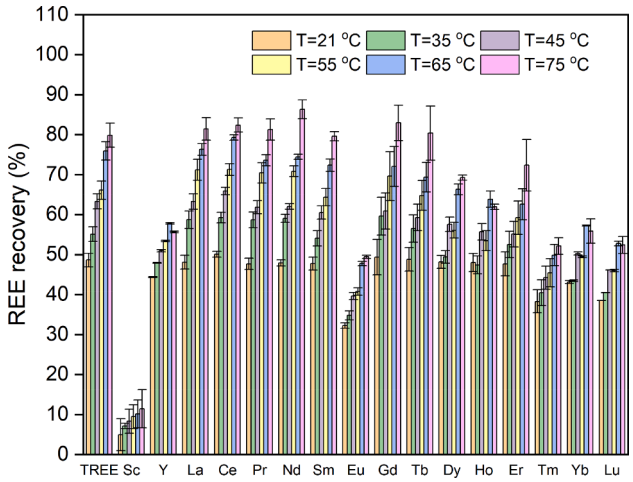

Fig. 4. Effect of leaching temperature on the REE recovery for the tests shown in Fig. 3e. Conditions: S/L ratio = 25 g/L, d_{80} = 47.9 μm, 1 M H_2SO_4, 21–75 °C, and 2 h. Note: error bars represent the standard deviations.

(K), respectively. The specific kinetic type can be determined by fitting leaching recoveries with the models (Jun et al., 2010). The apparent activation energy for a diffusion control is less than 20 kJ/mol, while the value for a chemical-controlled process normally exceeds 40 kJ/mol (Tan et al., 2016; Lee et al., 2005). The mix-controlled process, i.e., the coexistence of diffusion and chemical reaction mechanisms, usually has an activation energy of 20–40 kJ/mol (Brahim et al., 2022).

Since each leaching curve has two distinct stages, attempts were made to model the experimental data separately for each stage at different temperatures. A similar manner had been adopted by Yang and Honaker (2020) and Olvera-Venegas et al. (2017) to analyze the leaching kinetics of metals. The experimental data was evaluated by Eqs. (5-8). The involved kinetic parameters, including the apparent reaction rate (k), the intercept of the regressed line (b), and the adjusted coefficient of determination (R^2), are summarized in Table 3. Nearly all the R^2 of the regressed lines are larger than 0.9 if the leaching kinetic curves were modeled by dividing into 0–10 min and 10–120 min stages. However, the leaching process was less likely to be chemical reaction-controlled since the poor linearity (R^2 <0.9) of -lnK versus t and the small E_a values (<25 kJ/mol). Compared to chemical reaction control, the leaching recovery of a diffusion-controlled process is normally less temperature-dependent (Yang et al., 2014). This suggests that diffusion control is also not suitable given the temperature-dependent TREE recovery observed in Fig. 3e. As such, the optimal kinetic model that fits the leaching rate of REEs is likely the mix control.

Fig. 7a and -b show the plots of $[1-(1-x)^{1/3} + B[1-2x/3-(1-x)^{2/3}]]$ versus time in the two stages. It indicates that t = 10 min was a critical point at which the leaching rate began to decrease significantly. Fig. 8a and -b show the Arrhenius plots of -ln(k) versus 1000/T based on Fig. 7a and -b. The determined E_a value for the first (i.e., 0–10 min) and the second steps (10–120 min) is 20.3 (E_{a1}) and 10.8 kJ/mol (E_{a2}), respectively. In fact, the maximum possible activation energy required for the leaching of REEs in the second stage should be the summation of E_{a1} and E_{a2} (i.e., 31.1 kJ/mol), which belongs to the range of E_a (20-40 kJ/mol) used to differentiate the mix-controlled process.

4. Discussion

4.1. Passivation layer and leaching kinetics

The kinetic study suggests that the rate-determining step for the dissolution of REMs from the feed sample by H_2SO_4 was governed by the chemical reactions on the solid/liquid interface and the transportation of the reactants to the bulk solution. However, it is still not clear about the significantly decreased leaching rate after 10 min. One possible reason may be the formation of a passivation layer.

The content of Ca in the feed sample was 9766.7 ppm (see Table 2). Assuming all the Ca was dissolved during the leaching, the maximum concentration of Ca in the leachate would be 0.098 g/L, which is lower than the one (0.818 g/L) estimated based on the solubility of $CaSO_4$ in 1 M H_2SO_4 at 25 °C (Cameron and Breazeale, 2002). Therefore, the precipitation of Ca as $CaSO_4$ during the leaching process was not possible.

Another possible passivation layer formed during the leaching process may be silica gel since the dominant minerals and the REE-bearing minerals were all silicates in the feed sample. Soluble silica exists as silicic acid (i.e., $Si(OH)_4$) at pH <7. Silicic acid molecules can combine with each other via Si-O-Si branches and produce polysilicic acid, which would further form colloids and then silica gel (Alkan et al., 2018). To explore the possibility of the formation of silica gel, a 40 mL of fresh H_2SO_4 solution was added to the leaching system that already had 40 mL lixiviant at t = 15 min, at which the leaching rate of REEs decreased significantly according to Fig. 3e. The additional lixiviant added halved the S/L ratio compared to the initial. The concentration of soluble Si should also be reduced, thereby decreasing the likelihood of the gelation of silicic acid into silica gel. If the formation of silica gel was responsible for the reduced leaching rate of REEs, a more rapid leaching rate was expected to appear after the addition of extra H_2SO_4 solution. However, the results presented in Fig. 9 show that the leaching curves at both temperatures still climbed slowly, which was similar to the characteristics observed in Fig. 3e. The SEM images of the feed sample before and after leaching are presented in Fig. 10. It shows that the surface morphology became smoother relative to the one before leaching due to the partial dissolution of the small chunks on the surface of each particle by proton attack, exposing the fresh surfaces underneath. The leaching results in Fig. 9 along with the SEM analysis revealed that the passivating effect of silica gel was less likely to explain the decreased leaching rate in the second stage (i.e., t = 10–120 min shown in Fig. 3e).

4.2. The crystallinity of allanite and the leaching kinetics

Since the formation of passivation layer was less likely to explain the reduced leaching rate after 10 min, it may be reasonable to explore whether the existence of difficult-to-leach REMs was the reason. As such, the leaching residue obtained at 75 °C by 1 M H_2SO_4 (i.e., the one shown in Fig. 3e) was re-leached by 1, 2, and 4 M H_2SO_4, respectively, under the same conditions. Fig. 11a illustrates that re-leaching the residue for another 2 h only led to the extraction of 6.8%–9.0% more REEs. When the re-leaching curves in Fig. 11a were plotted as the continuation of the initial leaching stage (see Fig. 11b), the TREE recovery continued to increase but with a leaching rate as slow as the one observed between 10 and 120 min in Fig. 3e. The highest final TREE recovery reached 86.2% using 4 M H_2SO_4. It suggested that the remaining REEs in the leaching residue may be associated with acid-resistant REMs, which can be gradually released using a stronger acid and extending the contact time.

Yang and Honaker (2020) extracted REEs from a Fire Clay coal seam using 1.2 M H_2SO_4 at 75 °C and found that the TREE leaching curves slowly increased after 20 mins. This leaching behavior was explained by the leaching of REE-bearing species with varying leachabilities. REEs in the readily leachable form, including ion-exchangeable, carbonate, and metal oxide forms, were instantaneously leached at the beginning of the extraction process, while releasing REEs from the difficult-to-leach forms was slower. This finding suggests that the leaching rate was affected by the varying leachability of REE-bearing species in the coal sample.

The results in Section 3.1 show that allanite was the dominant REM in the feed sample. Furthermore, the report by the American Rare Earths (2023) found that most of the allanite belonged to metamict allanite, an amorphous status resulting from the radiation damage of the radiogenic elements (e.g., Th and/or U) incorporated over geological timescales (Beirau et al., 2011; Reissner et al., 2019). The degree of structural

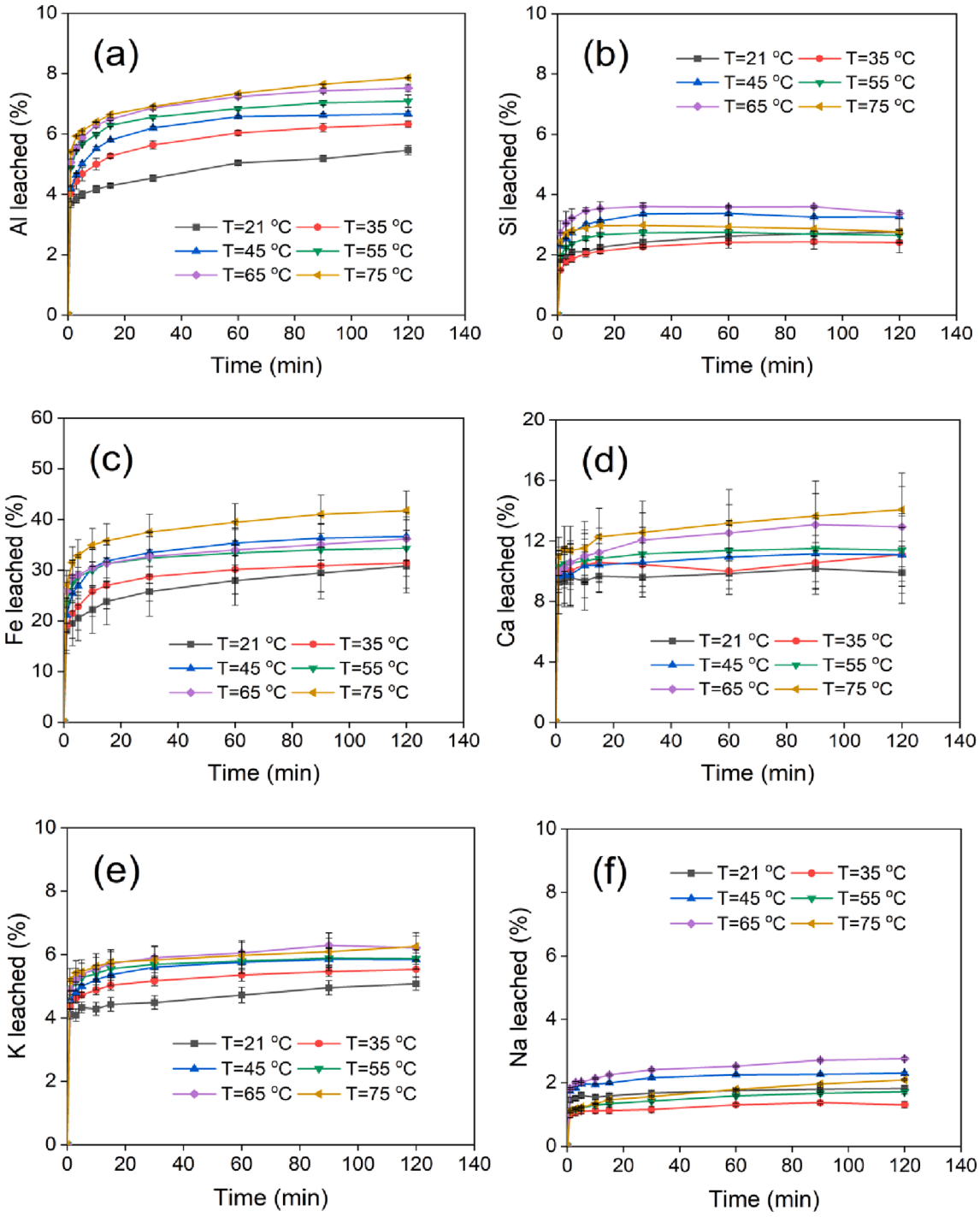

Fig. 5. Effect of leaching temperature on the fraction of the contaminant elements (Al, Si, Fe, Ca, K, and Na) leached from the feed sample. Conditions: S/L ratio = 25 g/L, d_{80} = 47.9 μm, 1 M H_2SO_4, 21–75 °C, and 2 h. Note: error bars represent the standard deviations.

damage ranges from single point-defects through intermediate stages up to fully amorphous status depending on the radiation dose (Ewing et al., 1987). For the amorphous REMs, which had more disordered crystal structures, the diffusion of acid inside the crystals was easier relative to the well-crystallized ones (Kim and Osseo-Asare, 2012; Granata et al., 2019; Kalinkin and Kalinkina, 2011). Thus, the well-crystallized allanite supposed to have poorer leachability compared to the ones in amorphous form. As such, it might be the existence of REMs resistant to acid leaching such as well-crystallized allanite that led to the distinct leaching kinetics observed in Fig. 3.

However, direct locating metamict allanite by transmission electron microscopy would be a difficult task considering the TREE content in the feed was only 9,861 ppm. Fortunately, one characteristic of metamict allanite is that the radiation-damaged crystal structure can be partially recrystallized by thermal annealing (Beirau et al., 2011; Janeczek and Eby, 1993), and the recrystallization starts at approximately 500 K (Reissner et al., 2019). As such, a series of H_2SO_4 leaching tests was performed on the feed sample calcined at varying temperatures (i.e., 300, 600, and 900 °C). Fig. 12 shows that the final TREE recovery gradually declined with the increase of calcination temperature when compared to the one without calcination. The decreased extraction was attributed to the enhanced conversion of metamict allanite to its more

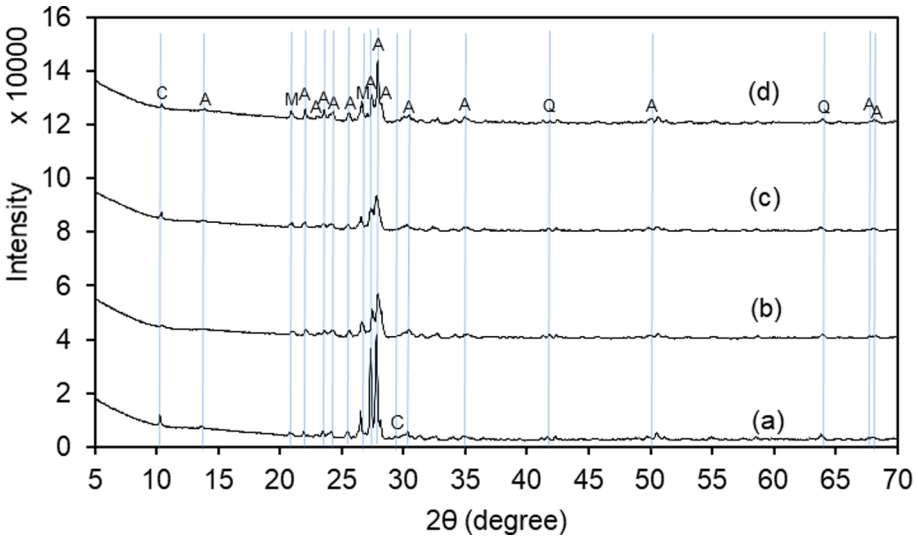

Fig. 6. X-ray diffraction (XRD) spectra of (a) allanite feed sample and the allanite feed sample leached by 1 M H_2SO_4 at (b) 35 °C, (c) 55 °C, and (d) 75 °C (A: Albite-$NaAlSi_3O_8$; M: microcline-$KAlSi_3O_8$; C: actinolite-$Ca_2(Mg_{4.5\text{-}2.5}Fe^{2+}_{0.5\text{-}2.5})Si_8O_{22}(OH)_2$; Q: quartz-$SiO_2$).

Table 3
The rate constants (k, min^{-1}), intercepts of the regressed line (b), and correlation coefficients (R^2) of leaching REEs from the feed sample using 1 M H_2SO_4 at various temperatures for 2 h (note: "temp." denotes temperature).

Inner diffusion control		1–10 min			10–120 min		
Temp. (°C)	Temp. (K)	k	b	R^2	k	b	R^2
21	294.15	0.00040	0.00106	0.9304	0.00018	0.02020	0.9347
35	308.15	0.00100	0.00980	0.9716	0.00020	0.01320	0.9970
45	318.15	0.00170	0.01270	0.9851	0.00031	0.03050	0.9410
55	328.15	0.00210	0.01780	0.9609	0.00031	0.03988	0.9238
65	338.15	0.00300	0.02450	0.9579	0.00050	0.05300	0.9523
75	348.15	0.00310	0.03060	0.9361	0.00060	0.06080	0.9658
Chemical reaction control		1–10 min			10–120 min		
Temp. (°C)	Temp. (K)	k	b	R^2	k	b	R^2
21	294.15	0.00200	0.10720	0.91930	0.00070	0.12250	0.99010
35	308.15	0.00440	0.10350	0.95390	0.00080	0.15150	0.91260
45	318.15	0.00660	0.11980	0.96920	0.00089	0.18830	0.92280
55	328.15	0.00730	0.14210	0.93860	0.00081	0.21690	0.90930
65	338.15	0.00890	0.16830	0.93640	0.00110	0.25420	0.94120
75	348.15	0.00880	0.18860	0.91300	0.00120	0.27470	0.95620
Mix control		1–10 min			10–120 min		
Temp. (°C)	Temp. (K)	k	b	R^2	k	b	R^2
21	294.15	0.00500	0.15150	0.90660	0.00160	0.18840	0.99460
35	308.15	0.00870	0.14640	0.96310	0.00170	0.23410	0.93640
45	318.15	0.01320	0.16930	0.97790	0.00210	0.30660	0.93370
55	328.15	0.01470	0.20400	0.95040	0.00220	0.36810	0.89530
65	338.15	0.01760	0.24100	0.94750	0.00260	0.41130	0.94760
75	348.15	0.01770	0.27550	0.92500	0.00280	0.44860	0.96040

difficult-to-leach forms (i.e., the crystallized allanite) at higher temperatures. This finding confirms the existence of metamict allanite. Therefore, the rapid leaching rate within the 0–10 min may result from the dissolution of the readily leachable REMs, such as metamict allanite, while the following slower leaching kinetics between 10 and 120 min was explained by the slow release of REEs from the remaining REMs, such as crystallized allanite, which were difficult to leach.

5. Conclusions

The present work investigated the extraction of REEs from an allanite ore containing 9,861 ppm of REEs using the direct acid leaching method. The EPMA-WDS and SEM-EDS characterization results confirmed the existence of allanite as the dominant REM in the feed sample, which mainly consisted of albite, microcline, and actinolite. Other REMs in minor amounts included synchysite/bastnasite and chevkinite/tornebohmite. Acid screening tests showed that H_2SO_4 is a superior lixiviant relative to HNO_3 and HCl since SO_4^{2-} may act as a stronger ligand to complex with REE^{3+}. Compared to the initial H_2SO_4 concentration and particle size, temperature and S/L ratio had greater impacts on the TREE recovery during the leaching process. XRD analysis of the leaching residues indicated that the leaching process did not lead to a massive decomposition of the gangue minerals.

Approximately 80% of the TREE recovery was obtained using 1 M

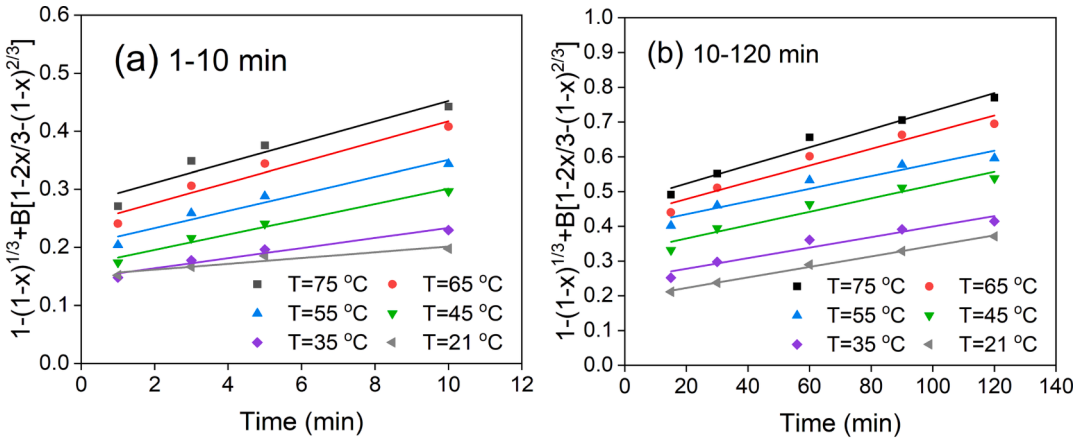

Fig. 7. Plots of $[1-(1-x)^{1/3} + B[1-2x/3-(1-x)^{2/3}]$ versus time for the leaching of REEs from the feed sample during the first 10 min (a) and 10–120 min (b) using 1 M H_2SO_4 at various temperatures for 2 h.

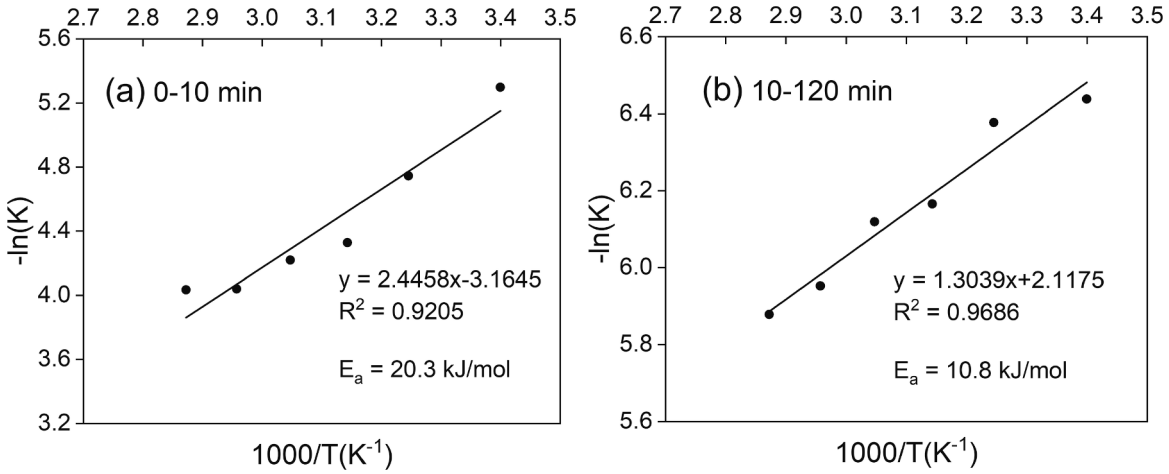

Fig. 8. Arrhenius plot for the leaching of REEs from the feed sample during the first 10 min (a) and 10–120 min (b) using 1 M H_2SO_4 at various temperatures for 2 h.

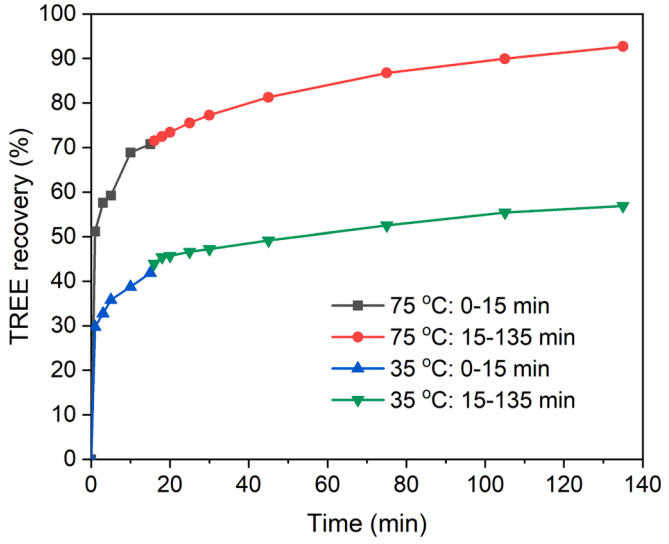

Fig. 9. Leaching characteristics of TREE from the feed sample by 1 M H_2SO_4 with a S/L ratio of 25 g/L for 135 min at 35 and 75 °C, respectively. A 40 mL 1 M H_2SO_4 solution pre-heated to the corresponding reaction temperature was added to the leaching system at t = 15 min since the start of the leaching.

H_2SO_4 at 75 °C for 2 h, demonstrating that most allanite could be dissolved by the acid at <100 °C. A common leaching characteristic of the REEs is that: the recovery underwent a rapid increase in the first 10 min, after which it slowly increased. The kinetic modeling revealed that the leaching rates of REEs at both stages were mix-controlled, i.e., a combination of both surface chemical reaction and diffusion through a product layer. The determined activation energies for the H_2SO_4 leaching of REEs in the first (0–10 min) and the second stage (10–120 min) are 20.3 and 10.8 kJ/mol, respectively.

The initial rapid leaching rate was more likely to be explained by the preferential leaching of REMs in amorphous forms, such as metamict allanite, which was readily leachable relative to its more crystallized ones. The presence of metamict allanite was indirectly confirmed by the reduced TREE recovery with the increase in the calcination temperature from 300 to 900 °C. The limited improvements in TREE recovery resulting from the particle size reduction of the feed sample also indicated the existence of well-crystallized REMs. The promising leaching recovery obtained in this study enables the allanite to be a promising feedstock for REEs.

CRediT authorship contribution statement

Wei Liu: Conceptualization, Methodology, Investigation, Writing – original draft. **Zhongqing Xiao:** Conceptualization, Investigation, Writing – review & editing. **Subodh Das:** Resources. **Wencai Zhang:** Supervision, Project administration, Funding acquisition, Writing –

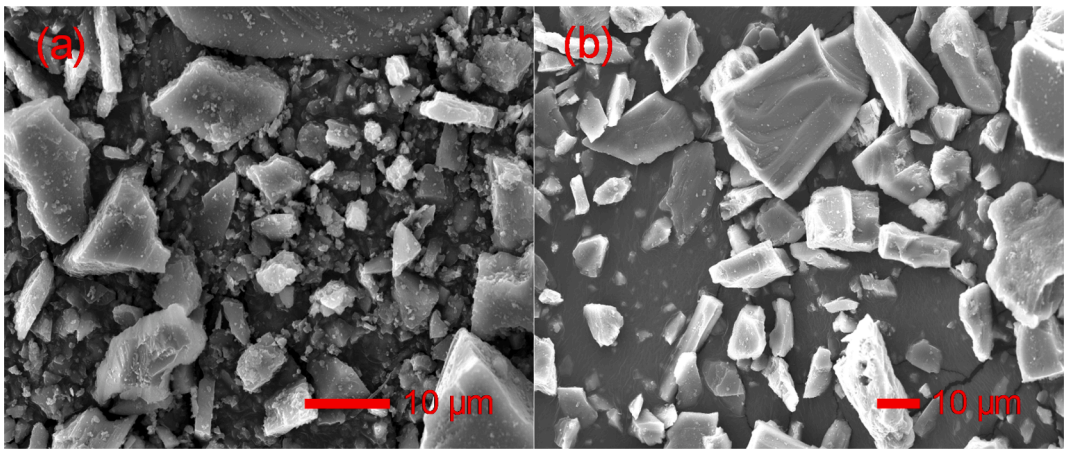

Fig. 10. Scanning electron microscopy (SEM) images of the feed sample before (a) and after 1 M H_2SO_4 leaching at 75 °C for 2 h with a S/L ratio of 25 g/L (b).

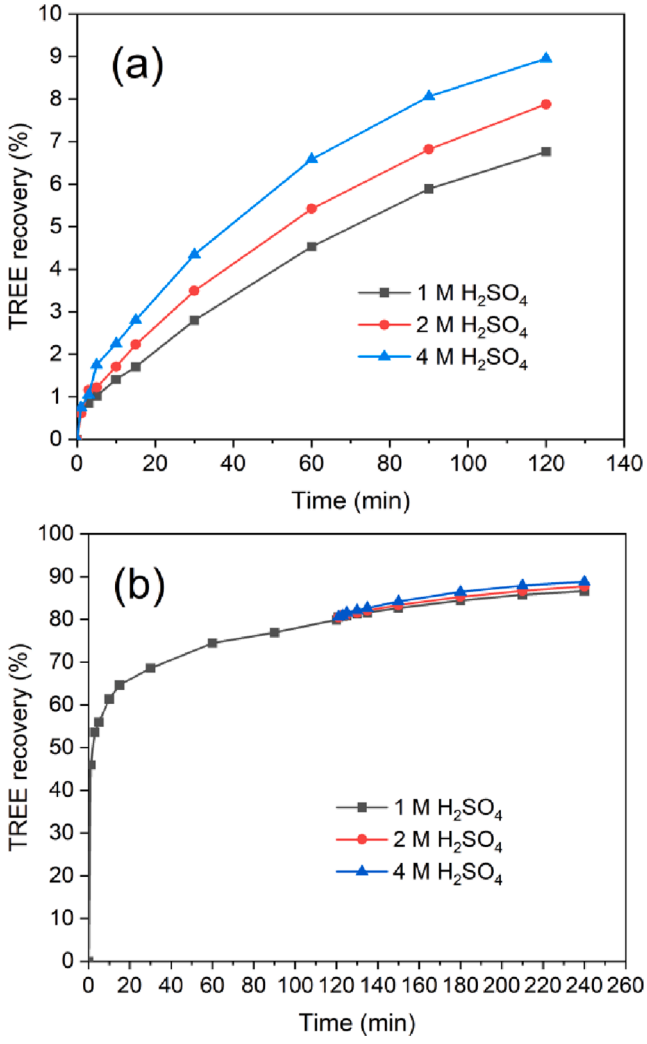

Fig. 11. Leaching characteristics of TREE from the leaching residue (obtained at 75 °C by 1 M H_2SO_4 for 2 h) using H_2SO_4 with different initial concentrations at 75 °C for 2 h, where (a) shows the TREE recovery only in the re-leach stage and (b) shows the cases in the initial leaching and re-leach stages (S/L ratio = 25 g/L).

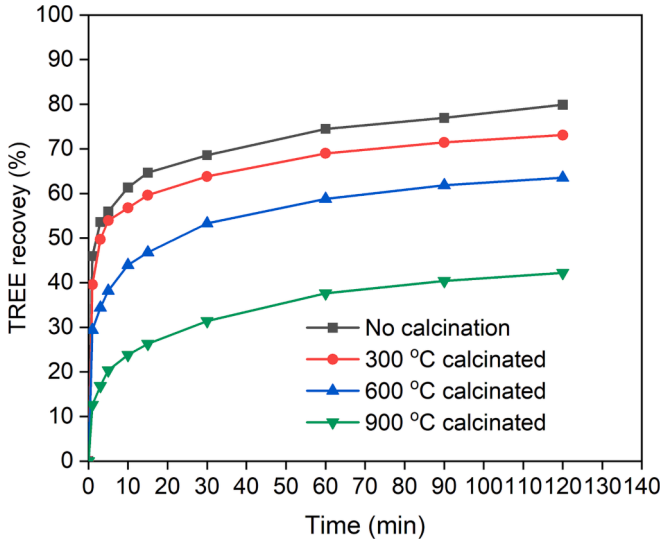

Fig. 12. Effect of calcination on the TREE recovery from the feed sample using 1 M H_2SO_4. Conditions: S/L ratio = 25 g/L, 75 °C, and 2 h.

review & editing.

Declaration of Competing Interest

The authors declare the following financial interests/personal relationships which may be considered as potential competing interests: Wencai Zhang reports financial support was provided by US Department of Energy.

Data availability

Data will be made available on request.

Acknowledgments

The authors thank Mohit Gupta for his suggestion and comments on kinetic model selection in this study. This material is based upon work supported by the U.S. Department of Energy's Office of Energy Efficiency and Renewable Energy (EERE) under the Advanced Manufacturing Office Award Number DE-EE0009435. Phinix, LLC is the primary recipient of this award.

Disclaimer: This report was prepared as an account of work sponsored by an agency of the United States Government. Neither the United

States Government nor any agency thereof, nor any of their employees, makes any warranty, express or implied, or assumes any legal liability or responsibility for the accuracy, completeness, or usefulness of any information, apparatus, product, or process disclosed, or represents that its use would not infringe privately owned rights. Reference herein to any specific commercial product, process, or service by trade name, trademark, manufacturer, or otherwise does not necessarily constitute or imply its endorsement, recommendation, or favoring by the United States Government or any agency thereof. The views and opinions of authors expressed herein do not necessarily state or reflect those of the United States Government or any agency thereof. Any opinions, finding, and conclusions or recommendations expressed in this publication are those of the author(s) and do not necessarily reflect the views of Phinix, LLC.

References

Alkan, G., Yagmurlu, B., Cakmakoglu, S., Hertel, T., Kaya, Ş., Gronen, L., Stopic, S., Friedrich, B., 2018. Novel approach for enhanced scandium and titanium leaching efficiency from bauxite residue with suppressed silica gel formation. Sci. Rep. 8 (1), 5676.

American Rare Earths 2023. Technical Report of Exploration and Maiden Resource Estimates of the Halleck Creek Rare Earths Project. https://americanrareearths.com.au/wp-content/uploads/2023/03/Halleck_Creek_Technical_Report_Appendices19.pdf.

Baillie, M.G., Hayton, J.D., 1970. In: A process for the recovery of high grade rare earth concentrates from Mary Kathleen uranium tailings. Institution of Mining and Metallurgy, London, pp. 334–345.

Balaram, V., 2023. Potential future alternative resources for rare earth elements: Opportunities and challenges. Minerals 13 (3), 425.

Beirau, T., Paulmann, C., Bismayer, U., 2011. Recrystallization of metamict allanite. Mineral. Mag. 75 (4), 2393–2399.

Benaouda, R., Kraemer, D., Bejtullahu, S., Mouttaqi, A., Bau, M., 2022. Occurrence of high-grade LREE allanite-pegmatites and calcite carbonatite dykes in the Ediacaran complex of Aghracha, Oulad Dlim massif (South Morocco). J. Afr. Earth Sc. 196, 104727.

Brahim, J.A., Hak, S.A., Achiou, B., Boulif, R., Beniazza, R., Benhida, R., 2022. Kinetics and mechanisms of leaching of rare earth elements from secondary resources. Miner. Eng. 177, 107351.

Cameron, F.K., Breazeale, J.F., 2002. Solubility of calcium sulphate in aqueous solutions of sulphuric acid. J. Phys. Chem. 7 (8), 571–577.

Cen, P., Bian, X., Liu, Z., Gu, M., Wu, W., Li, B., 2021. Extraction of rare earths from bastnaesite concentrates: A critical review and perspective for the future. Miner. Eng. 171, 107081.

Chakhmouradian, A.R., Wall, F., 2012. Rare earth elements: minerals, mines, magnets (and more). Elements 8 (5), 333–340.

Demol, J., Ho, E., Soldenhoff, K., Senanayake, G., 2019. The sulfuric acid bake and leach route for processing of rare earth ores and concentrates: A review. Hydrometall. 188, 123–139.

Dreisinger, D.B., Clucas, J.D., Verbaan, N., Grammatikopoulos, T., Aghamirian, M., Forstner, C., 2012. The processing of REE's from search minerals foxtrot resource. Proc. Rare Earths 81–94.

Edahbi, M., Plante, B., Benzaazoua, M., 2019. Environmental challenges and identification of the knowledge gaps associated with REE mine wastes management. J. Clean. Prod. 212, 1232–1241.

Ewing, R.C., Chakoumakos, B.C., Lumpkin, G.R., Murakami, T., 1987. The metamict state. MRS Bull. 12 (4), 58–66.

Georgiou, D., Papangelakis, V.G., 1998. Sulphuric acid pressure leaching of a limonitic laterite: chemistry and kinetics. Hydrometall. 49 (1–2), 23–46.

Gieré, R., Sorensen, S.S., 2004. Allanite and other REE-rich epidote-group minerals. Rev. Mineral. Geochem. 56 (1), 431–493.

Granata, G., Takahashi, K., Kato, T., Tokoro, C., 2019. Mechanochemical activation of chalcopyrite: Relationship between activation mechanism and leaching enhancement. Miner. Eng. 131, 280–285.

Gupta, T., 2021. Oxidation Pretreatment for Enhanced Leachability of Rare Earth Elements from Bituminous Coal Sources (Doctoral dissertation. University of Kentucky).

Gupta, C.K., Krishnamurthy, N., 1992. Extractive metallurgy of rare earths. Int. Mater. Rev. 37 (1), 197–248.

Jackson, W.D., Christiansen, G., 1993. International Strategic Minerals Inventory Summary Report–rare-earth Oxides, No. 930. US Government Printing Office.

Janeczek, J., Eby, R.K., 1993. Annealing of radiation damage in allanite and gadolinite. Phys. Chem. Miner. 19 (6), 343–356.

Jordens, A., Marion, C., Kuzmina, O., Waters, K.E., 2014. Physicochemical aspects of allanite flotation. J. Rare Earths 32 (5), 476–486.

Jun, T., Jingqun, Y., Ruan, C., Guohua, R., Mintao, J., Kexian, O., 2010. Kinetics on leaching rare earth from the weathered crust elution-deposited rare earth ores with ammonium sulfate solution. Hydrometall. 101 (3–4), 166–170.

Kalinkin, A.M., Kalinkina, E.V., 2011. Modelling of the sulfuric acid leaching of mechanically activated titanite. Hydrometall. 108 (3–4), 189–194.

Karan, R., Sreenivas, T., Babu, J.M., Kumar, M.A., Rao, K.A., Sahoo, H.S., Banerjee, A., Mundra, K.L., 2022. Hydrometallurgical Studies for the Recovery of Rare Earths from Micro-Granite Ore Deposit of Bhatikhera, Rajasthan, India. J. Geolog. Soc. India 98 (8), 1152–1158.

Kim, R., Cho, H., Han, K.N., Kim, K., Mun, M., 2016. Optimization of acid leaching of rare-earth elements from Mongolian apatite-based ore. Minerals 6 (3), 63.

Kim, E., Osseo-Asare, K., 2012. Aqueous stability of thorium and rare earth metals in monazite hydrometallurgy: Eh–pH diagrams for the systems Th–, Ce–, La–, Nd–(PO4)–(SO4)–H2O at 25 C. Hydrometall. 113, 67–78.

Krishnamurthy, N. and Gupta, C.K., 2015. Extractive Metallurgy of Rare Earths, ‖ CRC Press. Boca Raton, FL.

Kumari, A., Panda, R., Jha, M.K., Kumar, J.R., Lee, J.Y., 2015. Process development to recover rare earth metals from monazite mineral: A review. Miner. Eng. 79, 102–115.

Kursun, I., Terzi, M., Ozdemir, O., 2019. Determination of surface chemistry and flotation properties of rare earth mineral allanite. Miner. Eng. 132, 113–120.

Leal Filho, W., Kotter, R., Özuyar, P.G., Abubakar, I.R., Eustachio, J.H.P.P., Matandirotya, N.R., 2023. Understanding Rare Earth Elements as Critical Raw Materials. Sustainability 15 (3), 1919.

Lee, I.H., Wang, Y.J., Chern, J.M., 2005. Extraction kinetics of heavy metal-containing sludge. J. Hazard. Mater. 123 (1–3), 112–119.

Li, X., Xing, P., Du, X., Gao, S., Chen, C., 2017. Influencing factors and kinetics analysis on the leaching of iron from boron carbide waste-scrap with ultrasound-assisted method. Ultrason. Sonochem. 38, 84–91.

Li, M., Zhang, X., Liu, Z., Hu, Y., Wang, M., Liu, J., Yang, J., 2013. Kinetics of leaching fluoride from mixed rare earth concentrate with hydrochloric acid and aluminum chloride. Hydrometall. 140, 71–76.

Liu, W., Feng, X., Noble, A., Yoon, R.H., 2022. Ammonium sulfate leaching of NaOH-treated monazite. Miner. Eng. 188, 107817.

Mao, F., Zhu, N., Zhu, W., Liu, B., Wu, P., Dang, Z., 2022. Efficient recovery of rare earth elements from discarded NdFeB magnets by mechanical activation coupled with acid leaching. Environ. Sci. Pollut. Res. 1–12.

Mariano, A.N., Mariano, A., 2012. Rare earth mining and exploration in North America. Elements 8 (5), 369–376.

Millero, F.J., 1992. Stability constants for the formation of rare earth-inorganic complexes as a function of ionic strength. Geochim. Cosmochim. Acta 56 (8), 3123–3132.

Moldoveanu, G.A., Papangelakis, V.G., 2012. Recovery of rare earth elements adsorbed on clay minerals: I. Desorption mechanism. Hydrometallurgy 117, 71–78.

Olvera-Venegas, P.N., Cruz, L.H., Lapidus, G.T., 2017. Leaching of iron oxides from kaolin: Synergistic effect of citrate-thiosulfate and kinetic analysis. Hydrometall. 171, 16–26.

Panteeva, S.V., Gladkochoub, D.P., Donskaya, T.V., Markova, V.V., Sandimirova, G.P., 2003. Determination of 24 trace elements in felsic rocks by inductively coupled plasma mass spectrometry after lithium metaborate fusion. Spectrochim. Acta B At. Spectrosc. 58 (2), 341–350.

Reissner, C.E., Bismayer, U., Kern, D., Reissner, M., Park, S., Zhang, J., Ewing, R.C., Shelyug, A., Navrotsky, A., Paulmann, C., Škoda, R., 2019. Mechanical and structural properties of radiation-damaged allanite-(Ce) and the effects of thermal annealing. Phys. Chem. Miner. 46, 921–933.

Tan, Q., Deng, C., Li, J., 2016 Jan 28. Innovative application of mechanical activation for rare earth elements recovering: process optimization and mechanism exploration. Sci. Rep. 6 (1), 19961.

Thibault, Y., Gamage McEvoy, J., 2020. Minimizing the impact of passivation during allanite-(Ce) decomposition in sulfuric acid media for rare earth recovery. Mineral. Petrol. 114, 559–571.

Tzifas, I.T., Papadopoulos, A., Misaelides, P., Godelitsas, A., Göttlicher, J., Tsikos, H., Gamaletsos, P.N., Luvizotto, G., Karydas, A.G., Petrelli, M., Noli, F., 2019. New insights into mineralogy and geochemistry of allanite-bearing Mediterranean coastal sands from Northern Greece. Geochemistry 79 (2), 247–267.

Yang, X., Honaker, R.Q., 2020. Leaching kinetics of rare earth elements from fire clay seam coal. Minerals 10 (6), 491.

Yang, Z., Li, H.Y., Yin, X.C., Yan, Z.M., Yan, X.M., Xie, B., 2014. Leaching kinetics of calcification roasted vanadium slag with high CaO content by sulfuric acid. Int. J. Miner. Process. 133, 105–111.

Yu, J., Guo, Z., Tang, H., 2013. Dephosphorization treatment of high phosphorus oolitic iron ore by hydrometallurgical process and leaching kinetics. ISIJ Int. 53 (12), 2056–2064.